Biochimica et Biophysica Acta, 1023 (1990) 389–397
Elsevier

BBAMEM 74809

Attraction, deformation and contact of membranes induced by low frequency electric fields

Dimiter S. Dimitrov *, Mariana A. Apostolova and Arthur E. Sowers

American Red Cross, Holland Laboratory / Cell Biology, Rockville, MD (U.S.A.)

(Received 23 October 1989)

Key words: Membrane; Erythrocyte ghost; Electric field; Cell attraction; Membrane deformation; Membrane contact; Dielectrophoresis; Kinetics

The force of attraction between erythrocyte ghosts induced by low frequency electric fields (60 Hz) was measured as a function of the intermembrane separation. It varied from 10^{-14} N for separation of the order of the cell diameter to 10^{-12} N for close approach and contact in 20 mM sodium phosphate buffers (conductivity 260 mS/m, pH 8.5). For large separations the interaction force followed a dependence on separation as predicted for dipole–dipole interactions. For small separation an empirical formula was obtained. The membranes deformed at close approach (< 1 μm) before making contact. The contact area increased with time until reaching the final equilibrium state. The ghosts separated reversibly after switching off the electric field. The membrane tension induced by the ghost interaction at contact was estimated to be of the order of 0.1 mN/m. These first quantitative measurements of the force/separation dependence for intermembrane interactions induced by low frequency electric fields indicate that attractive forces, membrane deformation and contact area of cells depend strongly on intermembrane separation and field strength. The quantitative relationships between them are important for measuring membrane surface and mechanical properties, intermembrane forces and understanding mechanisms of membrane adhesion, instability and fusion in electric fields and in general.

1. Introduction

Electric fields can induce cell attraction, deformation and aggregation by a phenomenon called dielectrophoresis [1–3]. In suspension of high cell concentration they lead to alignment of cells into long rows of chains of cells, the so-called 'pearl chains'. When cells are in contact, application of high-voltage DC pulses can induce cell fusion [4,5]. In many cases the close apposition of membranes is achieved by AC fields [4]. The role of the high-voltage DC pulse is to destabilize the membranes. It can also induce further membrane approach to reach molecular contact and membrane merging [6]. One way to examine the role of membrane approach and the forces of attraction, induced by electric fields, in the mechanisms of membrane fusion is to measure the rate of approach and the force of attraction which brings the membranes at close apposition. One of the difficulties in performing such experiments is to relate the rate of approach to the force and to control precisely the force. In this work we make use of an interpolation formula which relates the force which drives two spherical particles towards each other to the rate of mutual approach [7]. One basic advantage of using electric fields as a tool for studying mechanisms of membrane fusion is that they can be precisely controlled. For example, by changing the strength of the applied electric field one can control the driving force. This work proposes a method for measuring the intermembrane force of interaction induced by electric fields.

Several theoretical works aimed to calculate the force between membranes induced by electric fields [1,2,8]. Commonly, the force is represented as due to interaction of induced dipoles. Then the dipole moment induced by the field is calculated as a function of the system parameters such as cell radii, surface charge, medium conductivity and permitivity. The approach of induced dipole–dipole interactions fails to describe the intermembrane force at small intermembrane separations. In this case exact solutions of the electrostatic problem must be used. In addition, possible membrane bending deformations should be taken into account.

There are no experimental data on the force/distance dependence to compare with the theoretical predictions.

* Permanent address: Central Laboratory of Biophysics, Bulgarian Academy of Sciences, Sofia 1113, Bulgaria.

Correspondence: A.E. Sowers, American Red Cross, Holland Laboratory/Cell Biology, 15601 Crabbs Branch Way, Rockville, MD 20855, U.S.A.

The existing experimental data are mainly for colloid particles [2,9,10]. The recent experimental study of protoplast interactions induced by high-frequency (MHz range) electric fields [11] showed how the patterns of the electric fields could be revealed, but actually did not measure the force of attraction.

Use of an alternating electric field in the radio frequency range to induce cell contact necessary for electrofusion has been advocated for many years [4]. Recently, it was also shown that an AC field with a frequency as low as that available from the utility power lines (60 Hz) can induce attraction between cells and that this attraction can be used in cell electrofusion [5,12]. From a practical point of view this approach has the advantage that it greatly simplifies the apparatuses. From a theoretical point of view the cell interactions induced by AC fields in the radio-frequency range (0.1 to 10 MHz) are qualitatively different to that induced by low-frequency AC fields (10 Hz to 10 kHz) [13]. While in the former case the bulk of the cell is responsible for the force of attraction, in the case of low-frequency fields the cell–cell interaction is due to surface properties, mainly to the polarization of the double layer of counter-ions around the cell [10,14]. In a rigorous study of cell dielectrophoresis Chizmadzev et al. [8] derived theoretical formulas for both regions and presented estimates for the limits of validity of each approximation (bulk vs. surface). Dukhin indicated that at low frequencies it is likely that other effects due to non-equilibrium surface processes may occur [10]. In spite of the different physical mechanisms, the theoretical considerations predict that the radio-frequency AC electric field can lead to the same maximum driving force as the low-frequency fields do – that is the force at the maximum cell polarization. For cells in radio-frequency AC fields this corresponds to the requirement that the conductivity of the internal content of the cell be much higher than the conductivity of the medium. For low-frequency fields it is the surface charge which should be much higher than the parameter produced by the medium conductivity.

The main goal of this work is to measure the force/separation distance dependencies for approaching membranes induced by low-frequency electric fields. We also study the accompanying phenomena as membrane deformation and formation of contact. We emphasize the use of low-frequency electric fields, which has not been appreciated until recently. The results are important for understanding mechanisms of interaction of membranes in low-frequency electric fields, particularly membrane approach and fusion, characterization of membrane properties and for applications to biotechnology.

2. Materials and Methods

Cells and mediums

Human erythrocyte ghosts were obtained by hypotonic lysis [15], washed and stored in 20 mM sodium phosphate buffer (NaP_i) (pH 8.5, 4° C). The membranes were labeled with the fluorescent dye DiI (1,1′-dihexadecyl-3,3,3″,3′-tetramethylindocarbocyanine-perchlorate) (Molecular Probes, Oregon) as previously described [16]. Briefly, 0.01 ml of stock solution of DiI (3.5 mg/ml in absolute ethanol) was added while vortexing 1 ml of the buffer containing 0.1 ml of pelleted ghosts. After standing for 1 min, the excess DiI was removed by washing with 20 mM NaP_i buffer at $8000 \times g$ for 10 min at 0–4° C. The ghosts were stored as a pellet in refrigerator. The cell concentration in the suspension used for the experiments corresponded to an average distance between the ghost surfaces of the order of their diameters. Measurements were made on a total of 60 cells. Experiments were also performed with rabbit and sheep erythrocyte ghosts, in solutions of different buffer strength (5, 20 and 60 mM) and in solutions of increased viscosity (2.5 mPa · s), adjusted by adding glycerol (30% w/w).

Chamber and AC field

All observations were made with a rectangular chamber described in Ref. 17. The AC field frequency was 60 Hz and the field strength was 8 V/mm and 16 V/mm (16 V (r.m.s.) and 32 V (r.m.s.) applied across 2 mm chamber length). The experiments were performed at room temperature (22° C).

Fluorescence microscopy and TV video system

The observations were made using a Zeiss model 14 microscope and recorded on video tape in real time using a Zeiss three stage low light level Venus camera for subsequent single frame playback and analysis. The overall system contrast transfer function and its linearity was determined as a function of specimen location in the viewing field by the use of a series of cytometer fluorescent calibration spheres by Epics (Hialeah, FL) [18]. The separation distance, membrane deformation, contact area and cell size were measured by a Colorado Video (Boulder, CO) Model 321 analyzer. For several cases where the separation at small distances was difficult to measure, the intensity at all points on the scan line was also traced out on the strip chart recorder with intensity as a function of location on the screen. A Panasonic (Secaucus, NJ) NV-9300A and Colorado Video (Boulder, CO) Model 499 Video Multimemory were used to examine single frames of video sequences. A FORA (West Newton, MA) model VTG-22 video timer operated in the stopwatch mode placed an alpha numeric field with date and time information with ±0.01 s frame-to-frame accuracy onto each recorded video frame. The magnification was determined with a Lafayete objective micrometer and fluorescent calibration spheres. The experimental error in measuring the separation distance did not exceed 0.3 μm. We used

fluorescence microscopy instead of phase contrast for two reasons: (i) it is important to measure attraction forces between labeled membranes, because these are the membranes used for electrofusion in our experiments and (ii) the fluorescence technique avoids some of the problems of the phase contrast, such as interference rings and other diffraction phenomena.

Protocols and data processing

The chambers were filled with a 0.003 ml ghost suspension. Before every experiment the ghost membranes were examined under phase contrast. Then the electric field was applied and the image recorded. The motion and deformation of the DiI-labeled ghosts were recorded and analyzed by single frame play back of video sequences. The rate of approach was calculated by graphical differentiation of the separation vs. time dependencies. The attraction force was calculated by using an interpolation formula for the rate of approach of two spherical membranes at arbitrary separations [7].

3. Results

Main stages of approach, deformation and contact of membranes

Fig. 1 shows an example of the attraction which is induced by electric fields between erythrocyte ghosts. Our observations revealed the following qualitative features of the process:

(1) The AC field induces approach, deformation and contact of erythrocyte ghosts in 20 mM sodium phosphate buffer (Fig. 1).

(2) The rate of approach, the extent of deformation and contact area increase with field strength.

(3) The membranes change their spherical shape (i.e., they begin to deform) before making contact. There are two basic types of shape changes. Commonly the membranes flatten (see the membranes, denoted with *, just below the alphanumerics in the first frame of Fig. 1, time 02:25:32). In few cases a small elongation appears before making the contact (membranes, denoted with arrows, at the bottom right side of the third frame of Fig. 1, time 02:30:28).

(4) The contact area expands until reaching the final equilibrium state (Fig. 1, the membranes at the bottom right side of the fourth, fifth and sixth frames corresponding to times 02:30:93, 03:31:18 and 02:31:80).

(5) The cells become visibly separated within a time interval of the order of 1 minute after switching of the field.

(6) The separated cells can approach and make contact again after applying the field. This can be repeated as long as heating and evaporation damage irreversibly the cells and change the solute concentration. Therefore, the approach and contact are reversible.

(7) All basic observations for two interacting cells are essentially the same as for several interacting cells leading to pearl chain formation (see the two doublets of cells, denoted with *, below the alphanumerics of Fig. 1 which approach each other first to third frame, to form a pearl chain, fourth to sixth frame).

Fig. 2 shows schematically three basic stages of interactions of ghosts induced by electric fields: (a) approach of spherical membranes, (b) membrane deformation and (c) formation and expansion of the contact area. All the parameters which are denoted on the figure were measured as a function of time.

Separation distance and attraction force

Fig. 3 shows experimental data for the dependence of the separation, h, between the surfaces of human ghosts as a function of time, t, for two field intensities: 8 V/mm and 16 V/mm. The separation decreases with increasing time. The rate of decrease is very high just before making contact. The increase in field intensity leads to a decrease in time needed to travel the same distance.

The interaction force, F, calculated from the data shown in Fig. 3, sharply increases with a decrease in the separation distance (Fig. 4). The force increases with increasing the voltage. Figs. 5 and 6 show plots of the force vs. $1/(R_1 + R_2 + h)^4$ and log F vs. log h, respectively. In both cases there are two regions where the functional dependence of the force on the separation changes significantly. For large separations the force is proportional to $1/(R_1 + R_2 + h)^4$ (Fig. 5). The slope of the line for field intensity 16 V/mm ($8.3 \cdot 10^{-34}$ N $\cdot$ m^4) is almost 4-times larger than that for 8 V/mm ($2.2 \cdot 10^{-34}$ N $\cdot$ m^4). These two facts indicate that the interaction is due to induced dipoles [2,8,10]. Therefore the force can be calculated as

$$F = gE^2/(R_1 + R_2 + h)^4 \quad (1)$$

where E is the electric field intensity and g is a measure for the cell polarizability. It is always positive. The value of g was found to be equal to $(3.2 \pm 0.3) \cdot 10^{-42}$ N $\cdot$ m^6/V^2. This value is an average for 40 cells. The deviation from the average value reflects variations in cell properties and in some cases effects of interactions with other cells and hydrodynamic flows due to heating and/or electrohydrodynamic forces. In few cases the shape of the curve presenting the force/separation dependencies differed significantly from that shown in Fig. 4. These cases need further studies.

For small separations log F is proportional to log h (Fig. 6). Therefore in this region the force F can be approximated as

$$F = Ah^n \quad (2)$$

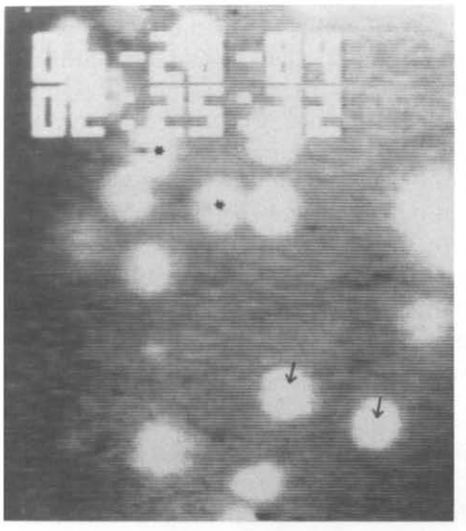

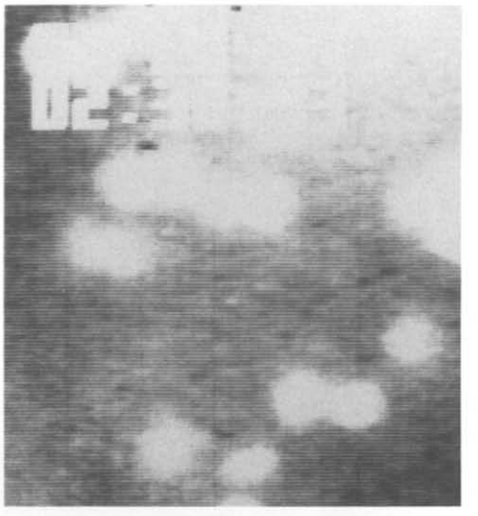

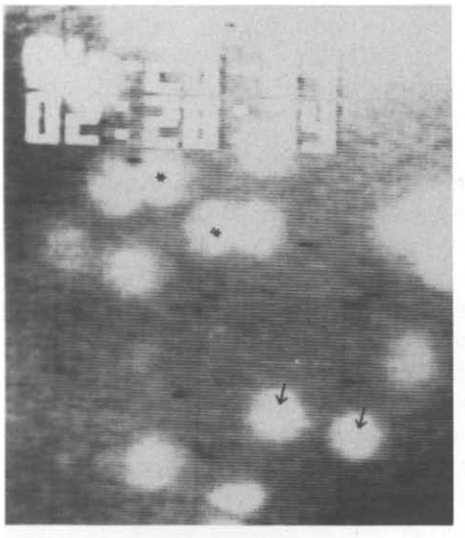

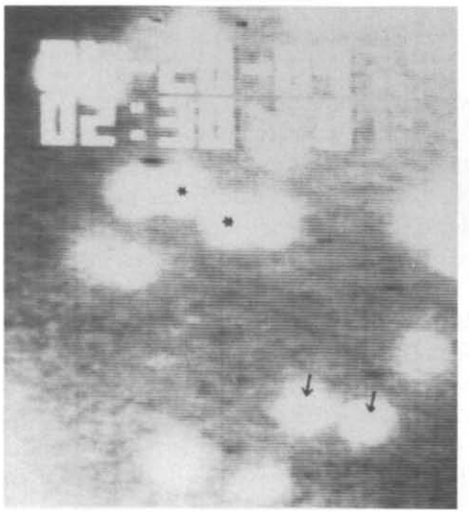

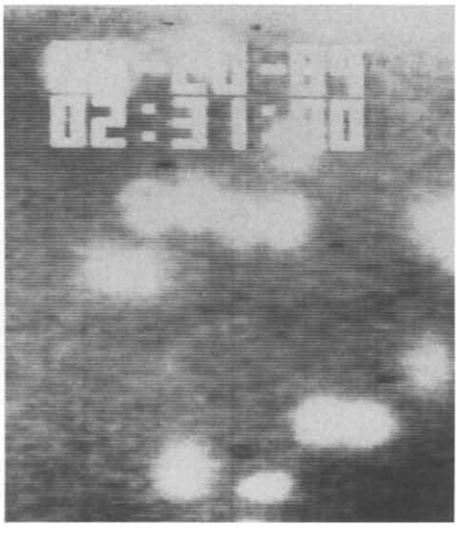

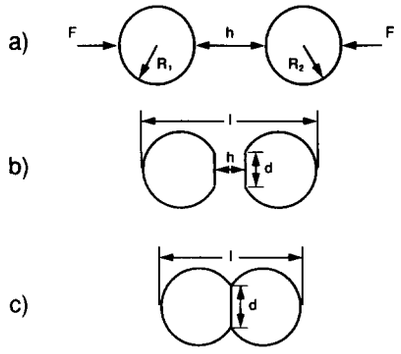

Fig. 2. Sketch of main stages of interactions of membranes (radii R_1 and R_2) in AC electric fields: (a) force (F)-induced approach of spherical membranes at large separations (h), (b) deformation of the membranes at close separation (before contact) and (c) contact and expansion of the contact area (with diameter d) until reaching an equilibrium state for which the distance between the ends of the cells (l) is smaller than the sum of their radii.

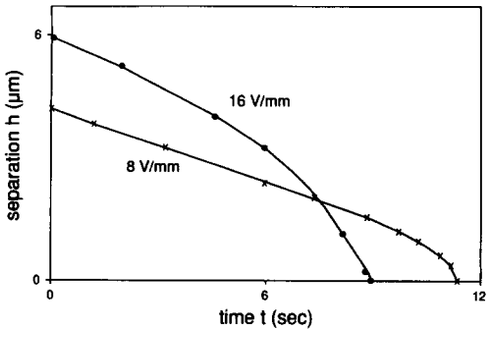

Fig. 3. Experimental data for the dependence of the separation distance, h, between the ghost surfaces with time t for two different electric field strengths, 8 V/mm and 16 V/mm. The time for the approach of two doublets of cells from the same initial distance to $h = 0$ is about 4-times longer for a field strength of 8 V/mm than for a field strength of 16 V/mm.

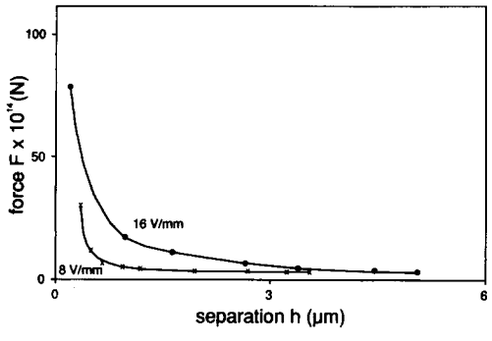

Fig. 4. Force of attraction between ghosts, F, as a function of separation h calculated from the data shown in Fig. 3. The force sharply increases at small separations.

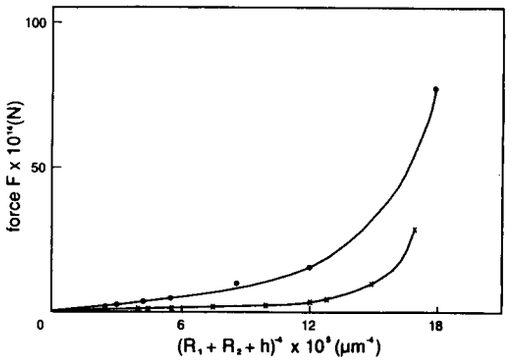

Fig. 5. Force of attraction, F, as a function of $(R_1 + R_2 + h)^{-4}$. The straight line which goes through zero for small forces represents a linear dependence which indicates that the force is due to the dipole–dipole interaction (see text). The slope of the straight line depends on the electric field intensity.

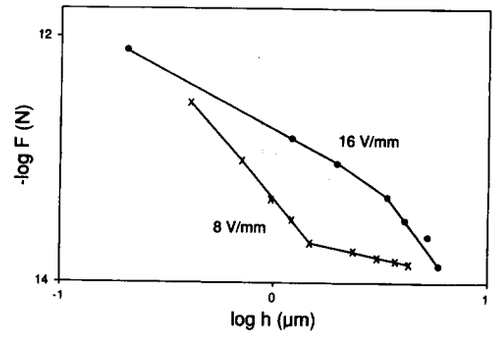

Fig. 6. Logarithmic plots of the force, F, as a function of separation h. The linear relationships permit to obtain empirical formulas for the attraction force at small separations.

where A and n are constants which do not depend on separation h. For field intensities 8 V/mm and 16 V/mm, $n = -1.84 \pm 0.18$ and $n = -1.08 \pm 0.24$; $\log A = -13.35 \pm 0.50$ and -12.75 ± 0.30, respectively (the dimensions are shown in Fig. 6). The membrane deformation for the higher voltage (16 V/mm) was relatively large at very small separations. At these separations the ghosts loose their spherical shapes. Therefore the force calculated by a formula valid for two sphere may not be a good approximation. This is probably the reason for the differences in the values of the constant n for both voltages.

Fig. 7 shows that there is good agreement between the experimental data for the force vs. separation dependencies and the formulas given by Eqns. 1 and 2

Fig. 1. Approach, deformation, contact and pearl chain formation of human erythrocyte ghosts in 60 Hz AC electric field of 16 V/mm intensity. Buffer in medium and cytoplasmic compartments is 20 mM NaP_i (pH 8.5). Alphanumerics: upper = date (month:day:year), lower = time (min:s:hundredths of s). The electric field is left-right and parallel to the plane of micrographs. It is applied at 02:25:00 (not shown). The width of the alphanumerics is exactly 50 μm. The two approaching ghosts, marked with arrows, at the lower right corner of the picture are spherical at large separations (02:25:32 and 02:28:39), they begin to deform at closer separations (02:30:28) and make contact (02:30:93), which expands (02:31:18) until reaching the final equilibrium state (02:31:80) where the radius does not change with time. One doublet of ghosts, marked with *, (below the alphanumerics) rotates (02:25:32) and approaches another doublet, marked with * (02:28:39). The two doublets make contact (02:30:28). The contact area expands and then does not change with time (02:30:93, 02:31:18 and 02:31:80).

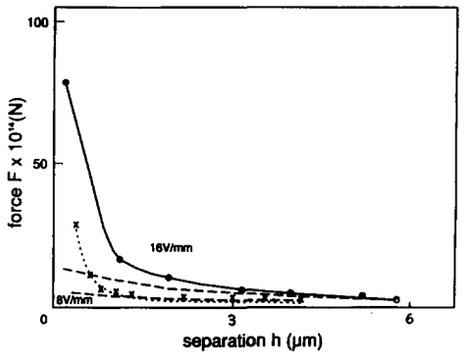

Fig. 7. Comparison between the experimental data for the dependence of the attraction force, F, shown in Fig. 5, and the dependencies calculated from the formula for dipole–dipole interaction (Eqn. 1) (— — —), valid for large separation) and the empirical formula (Eqn. 2) (·····, valid for small separation). The constants used are: $n = -2$, $A = 4.0 \cdot 10^{-20}$ N·m^2, and $g = 3.2 \cdot 10^{-42}$ N·m^6/V^2.

(the constants were evaluated from the linear dependencies shown in Fig. 5 and 6).

Membrane deformation, contact and separation

Fig. 8 shows the dependence of the separation l (see Fig. 2) and the diameter of the contact area as function of time. The dependence of the separation h on time is also shown for reference purposes. The separation distance l is a measure for the deformation of the membranes during their approach. For spherical membranes it must be always equal to the sum of the cell diameters and the separation between their surfaces h. It is seen from Fig.8 that it becomes smaller than the sum of the cell diameters before the separation h becomes zero. Therefore the membranes bend and begin to flatten

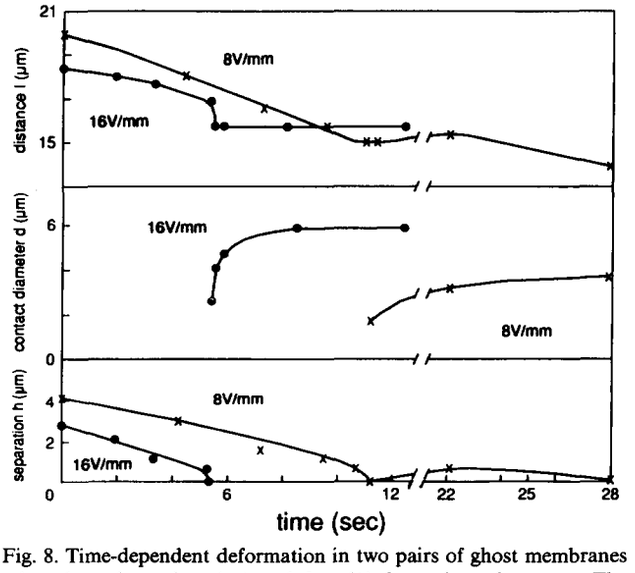

Fig. 8. Time-dependent deformation in two pairs of ghost membranes selected to show slow (×) and fast (●) formation of contact. The upper curves show the dependence of the separation l (see Fig. 2) on time. The lower curves are the separation h as function of time. The intermediate curves show how the diameter of the contact area increases with time until reaching the final static state.

before making contact. The extent of this deformation depends on the field strength and the membrane properties. Commonly with an increase in the field strength the deformation increases. The characteristic separation where the deviation from the spherical shape is measurable (i.e., is of the order of 1 μm) is of the order of 1–2 μm.

The formation of an almost plane-parallel liquid film between the membranes begins commonly hundreds of ms before making contact. Then the contact area expands (Fig. 8). The expansion continues for several seconds. In some cases it continues for tens of seconds as is seen in Fig. 8 for the one of the doublets of cells. In this case the contact between the cells is not strong enough. The cells separated for a couple of seconds (note the lowest curve at time = 22 s) before reaching the final equilibrium state. The diameters of the equilibrium contact area are of the order of 4–6 μm. They increase with field strength.

After switching off the electric field, the membranes usually separate within 10 to 60 s. In some cases it takes longer. The membranes always separated after removing the field. The separated membranes can be attracted towards each other again by applying the field again. The process of approach, induced by electric fields and separation, due to Brownian motion and electrostatic repulsive forces, is reversible. It can be repeated many times without any observable changes in the pattern of cell response. The characteristic features of formation of contact and separation can be changed only if the physicochemical environment is changed during application of the field, as heating of the cells and evaporation of water from the medium.

Effects of medium buffer strength and viscosity

The decrease of the buffer strength to 5 mM sodium phosphate led to decrease of the force. In 30% of the cases the cells did not make contact at field strength 8 V/mm. The force also decreased when the buffer strength was increased to 60 mM.

The average time of cell approach increased three times for interactions in 30% glycerol solutions (viscosity 2.5 mPa · s). The attraction force did not change significantly compared to the case without glycerol.

Rabbit and sheep erythrocyte ghosts

The attraction force between rabbit ghosts was slightly higher than for human, but not statistically significant because of the variation among individual cells. The sheep ghosts did not attract so strong as the human and rabbit did. At field strengths 8 V/mm 40% of the cells did not align at all.

4. Discussion

The results presented in this paper show that the attraction force between erythrocyte ghosts in low-

frequency alternating electric fields strongly depends on the separation between the membranes and the applied voltage. That force leads to membrane deformation at close approach and formation of area of flat membranes. Therefore, with respect to membrane shape changes, it is convenient to divide the mutual approach of membranes into three main stages:

(1) Approach of non-deformed (in our experiments, spherical), membranes.

(2) Bending deformation of the approaching membranes.

(3) Expansion of the contact area until the final equilibrium state is reached.

After switching off the electric field, the membranes separate. During separation, similar stages, but in reverse direction, occur.

There are several theoretical approaches to describe these phenomena. Commonly, the membranes are considered as spherical particles [1,8]. This leads to formulas for the attraction force essentially based on induced dipole–dipole interaction between spheres. The attempts to attack the problem for forces between deformed membranes induced by external electric fields lead to very complicated, untractable, and in most cases unsolvable, equations. On the other hand, there are approximate solutions for the shape and rate of approach of deformable membranes at given external driving force [7]. What follows below is: (i) a comparison of our experimental results for approach of spherical membranes with the predictions of the dipole–dipole interaction theory for the attraction force [1,8,10], (ii) a discussion of a possible empirical formula for the attraction force at close separation, (iii) a comparison of the observed onset of deformation with the theoretical prediction [7], and (iv) an estimation of the induced membrane tension on the basis of the experimental data for the attraction force. Unfortunately, there are no other quantitative measurements of the attraction force between membranes in low-frequency AC fields with which to compare with.

Approach of non-deformed membranes

The experimental observations have shown (see, e.g. Figs. 1, 8) that down to separation distance of approximately 1 μm, the membranes retain their spherical shape. The force of attraction F fits well the prediction of the theory for dipole–dipole at large separations as is seen in Fig. 6. The theory predicts that the polarizability coefficient g depends mainly on the surface charge, conductivity of the solution, permitivity of the medium and the radii of the cells [8,10]. It can be represented as

$$g = 24\pi\varepsilon R^6 x^2$$

where ε is the medium permitivity, R the cell radius and x the dimensionless polarizability. The dimensionless polarizability x is commonly given by [2,10]

$$x = [-1 + 3\,\mathrm{Rel}/(1 + \mathrm{Rel})]/2$$

The dimensionless group Rel can be approximated as qu/KR, where q is the surface charge density, u the electrophoretic mobility and K the volume conductivity [2]. For high surface charges x is equal to unity. For low and zero surface charge x equals $-1/2$. For the curves shown in Fig. 5 (assuming the permitivity of the medium $\varepsilon = 80 \times 8.85 \times 10^{-12}$ F/m^1), $x^2 = 0.011 \pm 0.002$. Therefore x equals $+0.10$ or -0.10. The medium conductivity K is relatively high ($K = 0.26$ S/m) and the surface charge q and electrophoretic mobility u are relatively low ($q = 0.01$ C/m^2 and $u = 2.6 \cdot 10^{-8}$ m$^2 \cdot$ V$^{-1} \cdot$ s^{-1} [19]). The parameter $\mathrm{Rel} = qu/KR$, which determines the relative contribution of the surface and bulk conductivity [2,10], is much smaller than unity. This indicates that $x = -0.10$. Increasing the surface charge or decreasing the conductivity will increase the value of the dimensionless polarizability. This will lead to a decrease in the force (at $x = -1/2$ to 0) and then to an increase in the force (at $x = 0$ to 1). Variations in attractive force can be due to variations in surface charge of different cells or to non-equilibrium effects. This can explain our observation that the variations of the attraction force among individual cells are large and that erythrocyte ghosts from different species (sheep and rabbit) behave differently with respect to their response to external electric fields. It is difficult at this stage of development of the theory to explain the observed maximum in dielectrophoretic force at 20 mM sodium phosphate buffer, which correlates with a maximum in the electrofusion yield [5]. One of the possible mechanism is the increased conductivity in 60 mM solutions which can lead to lower interaction forces. It was shown that the dielectrophoretic forces acting on single cells at low frequencies are sensitive to conductivity: the increase of conductivity causes a decrease in the force [3]. The decrease in the medium ionic strength can lead to an increase of the double layer of counter-ions and therefore to an electrostatic repulsion of a longer range which can keep apart the cells at low buffer strength (5 mM). Rigorous comparison with data on single-cell dielectrophoresis may be useful in understanding the mechanism of interaction forces at low frequencies. In this aspect the recent experiments of Kaler and Jones [3], using a levitation feedback control system, are very promising. It is difficult, however, to use directly their data because they are for protoplasts, which differ significantly from erythrocyte ghosts, with respect to the response to external electric fields.

For small separations the formula for the induced dipole–dipole interactions no longer holds. The solution of the respective equations is very complicated if impos-

sible. Therefore, we prefer to derive an empirical formula which can be used to estimate the attraction force. It is seen from Fig. 6 that for small separations the force F can be approximated by Eqn. 2. For low voltages (8 V/mm) this dependence is

$$F = A/h^2$$

where $A = 4.0 \cdot 10^{-20}$ N · m^2.

As is seen in Fig. 7, the agreement between the experimental data and the forces calculated by the empirical formula is very good.

The above formula may be extrapolated to very small separations. Assuming also that F should be proportional to the square of the field intensity one can estimate the force during the pulse. The value of the pressure (force per unit area) exerted by the pulse is of the order of 10^{10} N/m^2. This is the order of magnitude or even higher than the hydration forces [20]. Therefore, one can expect that the energy delivered by the pulse can overcome the hydration barrier and bring the membranes at molecular contact. This conclusion already reached for the case of electrofusion of protoplasts [21] needs further experimental confirmation.

Membrane deformation

The theory predicts that when two membranes approach each other they will deform when the separation between them, h, equals $F/4\pi T$, where T is the membrane tension [7]. The experimental data show (see Figs. 1, 8) that this characteristic separation is of the order of 0.3 to 1 μm. In this interval the driving force is of the order of 10^{-3} N. Therefore the membrane tension at the onset of deformation is of the order of 100 μN/m. This is a very small value. But it is one order of magnitude higher than that for which the membrane tension forces become comparable with the forces due to membrane bending elasticity. This allows the membrane to keep its spherical shape.

Membrane contact

There is no simple theoretical expressions to describe the evolution of membrane shape and formation of nearly flat membranes with the subsequent expansion of the contact area. In addition, it is impossible to measure the membrane separation with precision higher than 0.3 μm with the fluorescence microscopy technique. Therefore at the present stage of our knowledge definite conclusions about possible comparison between theory and experiment cannot be made. One can perform, however, some estimates from the integral balance of forces. A theoretical formula [7], shows that the force F is related to the final equilibrium contact area S a

$$F = (2T/R)S$$

where F, T and R are the respective values for the final equilibrium state. Assuming that the equilibrium separation is of the order of 10 nm [22] and that the force F is, respectively, four orders of magnitude higher than that at 1000 nm (if Eqn. 2 holds) one can obtain values for the membrane tension at the final equilibrium state of the order of 0.1 mN/m, which is relatively high. Even if this estimate is too approximate, the conclusion is that the membrane tension is increased by the interaction. Similar conclusion has already been reached for equilibrium contact between membranes without electric fields [23,24]. One can speculate that during the high voltage pulse application the membrane tension can become higher than 10 mN/m, which will lead to membrane rupture or other effects which depend on the mechanical properties of the erythrocyte membrane [25].

Separation

After removing the AC field the membranes separate due to two main effects: (1) the repulsive intermembrane interactions, mainly of electrostatic origin and (2) Brownian motion. Theoretical estimates based on expressions for electrostatic repulsion and Brownian type diffusion showed that typical times of separation are of the order of minutes which is in reasonable agreement with our experimental observations.

Relation to other work

The results presented in this paper are important for understanding physical mechanisms of intermembrane interactions in electric fields and related phenomena. They can be used in studies of electrostatic, van der Waals and hydration intermembrane forces [20], mechanical properties of membranes and membrane adhesion [23–25], membrane fusion [26–29], dielectric spectroscopy of suspensions [13] and cell dielectrophoresis and electrocoagulation [2,30–32].

Conclusions

This paper presents the first quantitative measurements of the kinetics of approach of deformable membranes induced by low frequency electric fields and force/separation distance dependence. The data are in reasonable agreement with existing theories and are important for the elucidation of the mechanism of membrane fusion, membrane interactions in electric fields, electrofusion and electroporation, and evaluation of surface and mechanical properties of membranes.

Acknowledgements

The expert technical assistance of Ms. Myoung Soon Cho is greatfully acknowledged. Support from Ameri-

can Red Cross (to D.S.D.) and ONR grant N00014-89-J-1715 (to A.E.S.).

References

1 Pohl, H.A. (1978) Dielectrophoresis, Cambridge University Press, London.
2 Dukhin, S.S., Estrella-Lopes, V.R. and Jolkovski, E.K. (1985) Electro-surface phenomena and electrofiltration, Naukova Dumka, Kiev.
3 Kaler, K.V.I.S. and Jones, T.B. (1990) Biophys. J. 57, 173–182.
4 Zimmermann, U. (1982) Biochim. Biophys. Acta 694, 227–277.
5 Sowers, A.E. (1989) in Electroporation and electrofusion in cell biology (Neumann, E., Sowers, A.E. and Jordan, C.A., eds.), pp. 229–256, Plenum Press, New York.
6 Dimitrov, D.S. and Jain, R.K. (1984) Biochim. Biophys. Acta 779, 437–468.
7 Dimitrov, D.S. (1983) Progr. Surface Sci. 14, 295–424.
8 Chizmadzhev, Yu.A., Kuzmin, P.I. and Pastushenko, V.P. (1985) Biolog. Membr. 2, 1147–1161.
9 Allan, R.S. and Mason, S.G. (1962) J. Colloid Sci. 17, 383–408.
10 Dukhin, S.S. (1980) Croat. Chem. Acta 53, 167–181.
11 Mehrle, W., Hampp, R., Zimmermann, U. and Schwan, H.P. (1988) Biochim. Biophys. Acta 939, 561–568.
12 Sowers, A.E. (1983) Biochim. Biophys. Acta 735, 426–428.
13 Schwan, H.P. (1989) in Electroporation and electrofusion in cell biology (Neumann, E., Sowers, A.E. and Jordan, C.A., eds.), pp. 3–21, Plenum Press, New York.
14 Dukhin, S.S. and Shilov, V.N. (1974) Dielectric phenomena and double layer in dispers systems and polyelectrolytes, Halsted Press, New York.
15 Dodge, J.T., Mitchell, C. and Hanahan, D.J. (1963) Arch. Biochem. Biophys. 100, 119–130.
16 Sowers, A.E. (1986) J. Cell Biol. 102, 1358–1362.
17 Sowers, A.E. (1984) J. Cell Biol. 99, 1989–1996.
18 Inoue, S. (1986) Video microscopy, Plenum Press, New York.
19 Heard, D.H. and Seaman, G.V.F. (1960) J. Gen. Physiol. 43, 635–654.
20 Rand, R.P., Fuller, N., Parsegian, V.A. and Rau, D.C. (1988) Biochemistry 27, 7711–7722.
21 Dimitrov, D.S. and Zhelev, D.V. (1988) Colloid Polymer Sci. 76, 26–31.
22 Stenger, D.A. and Hui, S.W. (1989) in Electroporation and electrofusion in cell biology (Neumann, E., Sowers, A.E. and Jordan, C.A., eds.), pp. 167–180, Plenum Press, New York.
23 Evans, E.A. and Skalak, R. (1980) Mechanics and thermodynamics of biomembranes, CRC Press, Boca Raton, FL.
24 Evans, E.A. (1980) Biophys. J. 30, 265–274.
25 Berk, D.A., Hochmuth, R.M. and Waugh, R.E. (1989) in Red blood cell membranes: structure, function, clinical implications (Agre, P. and Parker, J.C., eds.), pp. 423–454, Marcel Dekker, New York.
26 Blumenthal, R. (1987) Curr. Top. Membr. Transp. 29, 203–254.
27 Sowers, A.E. (1987) Cell fusion, Plenum Press, New York.
28 Ohki, S. (1987) in Cell fusion (Sowers, A.E., ed.), pp. 331–352, Plenum Press, New York.
29 Teissié, J., Rols, M.P. and Blangero, C. (1989) in Electroporation and electrofusin in cell biology (Neumann, E., Sowers, A.E. and Jordan, C.A., eds.), pp. 203–214, Plenum Press, New York.
30 Iglesias, F.J., Santamaria, C., Lopez, M.C. and Dominguez, A. (1989) in Electroporation and electrofusion in cell biology (Neumann, E., Sowers, A.E. and Jordan, C.A., eds.), pp. 37–57, Plenum Press, New York.
31 Lamprecht, I. and Mischel, M. (1989) in Electroporation and electrofusion in cell biology (Neumann, E., Sowers, A.E. and Jordan, C.A., eds.), pp. 23–35, Plenum Press, New York.
32 Stoicheva, N., Tsoneva, I. and Dimitrov, D.S. (1985) Z. Naturforsch. 40c, 735–739.